Structural phase transition and the electronic and magnetic properties of Sr_2FeMoO_6

O. Chmaissem,[1,2] R. Kruk,[1,3] B. Dabrowski,[1,2] D. E. Brown,[1,2] X. Xiong,[1,2] S. Kolesnik,[1] J. D. Jorgensen,[2] and C. W. Kimball[1]

[1]*Department of Physics, Northern Illinois University, DeKalb, Illinois 60115*

[2]*Materials Science Division, Argonne National Laboratory, Argonne, Illinois 60439*

[3]*Institute of Nuclear Physics, 31-342 Kraków, Poland*

(Received 10 November 1999; revised manuscript received 11 August 2000)

The nuclear and magnetic structures of Sr_2FeMoO_6 have been investigated using neutron powder diffraction and Mössbauer spectroscopy at temperatures between 10 and 460 K. Fe and Mo atoms are found to order on alternate sites, as expected, giving rise to a double-perovskite-type unit cell. Upon cooling, a structural phase transition from cubic $Fm\bar{3}m$ to tetragonal $I4/m$ occurs at ~400 K. In the tetragonal $I4/m$ structure as the temperature decreases, the FeO_6 and MoO_6 octahedra rotate continuously around the c axis by an angle of up to ~5.6°. In the $I4/m$ phase, the magnetic moments for Fe and Mo order ferrimagnetically. The Fe magnetic spins first align along the c direction and then rotate to an angle of ~54° with respect to the c axis; the refined Fe magnetic moment saturates at $\sim 4.3\mu_B$. Mössbauer spectroscopy measurements show that the average valence of Fe is intermediate between the high spin configuration values of Fe^{+2} and Fe^{+3}. The temperature dependence of the mean hyperfine field is in good agreement with the neutron-diffraction results and gives the same transition temperature.

INTRODUCTION

The recent observation of tunneling magnetoresistance up to room temperature in Sr_2FeMoO_6 (Ref. 1) has drawn considerable interest because of the material's high magnetic transition temperature $T_c(\sim 400\,\mathrm{K})$ and its potential as an alternative to the manganese compounds. In manganese oxides, colossal negative magnetoresistance is usually observed near the magnetic transition temperature of the material (T_c), which is typically below room temperature. The magnetoresistance becomes smaller as T_c increases to room temperature, thus making it difficult to fully exploit the potential of these materials.

Sr_2FeMoO_6 is an ordered double perovskite of the $A_2BB'O_6$ type with Fe and Mo atoms alternating on the B and B' sites, respectively. Several measurements[2–4] suggested that the valence states of Fe and Mo are 3+ and 5+, respectively. Magnetization measurements, for example, showed a net moment of $\sim 3-3.4\mu_B$ at 4.2 K (Ref. 4) consistent with an antiferromagnetic coupling between the Fe and Mo moments ($5-1=4\mu_B$). A ferromagnetic coupling would otherwise give rise to a much larger net moment of $6\mu_B$.

From x-ray-diffraction patterns, the structure of Sr_2FeMoO_6 was suggested to be either tetragonal $\sqrt{2}a_p \times \sqrt{2}a_p \times 2a_p$,[1,4] or tetragonal (pseudocubic) ($\approx 2a_p \times \approx 2a_p) \times \approx 2a_p$ (Refs. 2 and 5–7) (where a_p is the unit cell of the primitive perovskite). Recently, a cubic $Fm\bar{3}m$ structure, at 300 and at 2.8 K, has been proposed by García-Landa *et al.*[8] using neutron powder diffraction. However, details of the nuclear and magnetic structures and the oxygen behavior (locations, displacements, etc.), as a function of temperature, have not been described. According to García-Landa *et al.*,[8] the refined magnetic moment of Fe is $4.1\mu_B$ and Mo does not contribute to the magnetic intensities. The authors[8] suggest that the Mo electrons are itinerant.

With proper annealing, Sr_2FeMoO_6 samples can be made insulating,[1,4] semimetallic, or metallic, which is quite unusual because the charge ordering of the Fe^{+3} and Mo^{+5} ions is expected to give rise to insulating properties only. Delocalized Mo electrons or cation nonstoichiometry could explain the metallic behavior of the material. Sleight *et al.*[9] suggested that the Fe^{+3}-Mo^{+5} combination could be degenerate with the Fe^{+2}-Mo^{+6} combination and that this valence degeneracy could be at the origin of the metallic behavior. Insulating Sr_2FeMoO_6 samples were made metallic by post-annealing in vacuum-sealed quartz tubes (for 72 h at 1373 K),[4] and this behavioral change was alternatively explained as possibly due to the improvement of conductivity of the grain-boundary phase or to the homogenization of the composition of the sample.

In this paper, we report temperature-dependent neutron powder diffraction and Mössbauer spectroscopy results for a Sr_2FeMoO_6 sample exhibiting a magnetic transition at ~400 K and insulating behavior down to 4 K. The room-temperature structures of metallic and semimetallic Sr_2FeMoO_6 samples are also presented. We find that a structural phase transition occurs at T_c (~400 K for our sample) where the structure changes from cubic $Fm\bar{3}m$ to tetragonal $I4/m$. In the tetragonal $I4/m$ structure, the magnetic moment of Fe first aligns along the c axis at temperatures close to T_c and then rotates, as the temperature is lowered, to an angle of ~54° with respect to the c axis (roughly along the [111] direction). The refined magnetic moment for Fe saturates at $\sim 4.3\mu_B$ at the lowest temperatures and the magnetic moments for Fe and Mo are found to order ferrimagnetically.

SYNTHESIS AND CHARACTERIZATION

Precursors were made from stoichiometric amounts of $SrCO_3$, Fe_2O_3, and MoO_3. These were intimately ground and fired in air at 1273–1473 K for up to 7 days. A high-

TABLE I. Synthesis conditions for samples *A*, *B*, and *C*.

Precursor 1: Raw powders annealed in air at 1273 K (1 day); pelletized and reannealed at 1473 K (1 h)
Precursor 2: Raw powders annealed in air at 1273 K (2 days); pelletized and reannealed at 1273 K (4 days).

		TGA synthesis		
Sample	Precursor	Heating rate (degree/min.)	Temperature (K)	Time (h)
A Insulating	Precursor 1	1.2	1573	2
B Semimetallic	Precursor 2	1.2	1573	2.5
C Metallic	Precursor 2	1.2	1573	2

temperature thermogravimetric balance (Cahn TGA171) with samples of ~3 g was then used to synthesize the Sr_2FeMoO_6 phase *in situ*. Several thermal conditions and various reducing atmospheres were tried until best results were achieved. A gas mixture of 0.5–1 %H_2/Ar, heating to 1573 K at a rate of 1.2 degree/min, and natural cooling to room temperature yielded samples of high purity. The final dense pellets are dark blue and magnetic at room temperature. Details of the synthesis procedures employed in preparing samples for this study are listed in Table I. Three samples designated as *A*, *B*, and *C* (insulating, semimetallic, and metallic, respectively), were prepared and characterized by x-ray powder diffraction at room temperature, neutron powder diffraction between 13 and 460 K, resistivity and magnetoresistance measurements (4.2–350 K), dc magnetization measurements (4.2–400 K; 400 K is the upper limit for our instrument) using a Quantum Design Physical Properties Measurement System-Model 6000, and Mössbauer spectroscopy (10–460 K).

Mössbauer measurements were performed in transmission geometry with a 50 mCi ^{57m}Co in Rh source kept at room temperature and a krypton proportional detector. Measurements between 10 and 460 K were made in an exchange gas cryostat cooled with liquid nitrogen and helium. Rhodium-iron resistance sensors allowed the control and stabilization of the temperature to within ± 0.1 K.

Time-of-flight neutron powder diffraction data were collected on the Special Environment Powder Diffractometer[10] (SEPD) at the Intense Pulsed Neutron Source (IPNS). For sample *A*, diffraction data were acquired at 17 different temperatures between 13 and 460 K using a closed-cycle helium refrigerator with capabilities for heating above room temperature. For samples *B* and *C* only room-temperature diffraction data were collected. High-resolution back-scattering data, from 0.5 to 4 Å, were analyzed using the Rietveld technique with the General Structure Analysis System (GSAS) code.[11] In the analysis, background, peak width, and the extinction parameter were refined, together with the lattice parameters, oxygen atomic positions, and isotropic and anisotropic temperature factors for the cations and oxygen atoms, respectively.

RESULTS AND DISCUSSION

Resistive and magnetic properties

The synthesis conditions described in Table I result in high-quality samples. However, the conducting properties were found to depend sensitively on the precursor history and annealing time. Resistivity measurements at several magnetic fields as a function of temperature are shown in Fig. 1 for three samples having different conducting properties: insulating, semimetallic, and metallic (samples *A*, *B*,

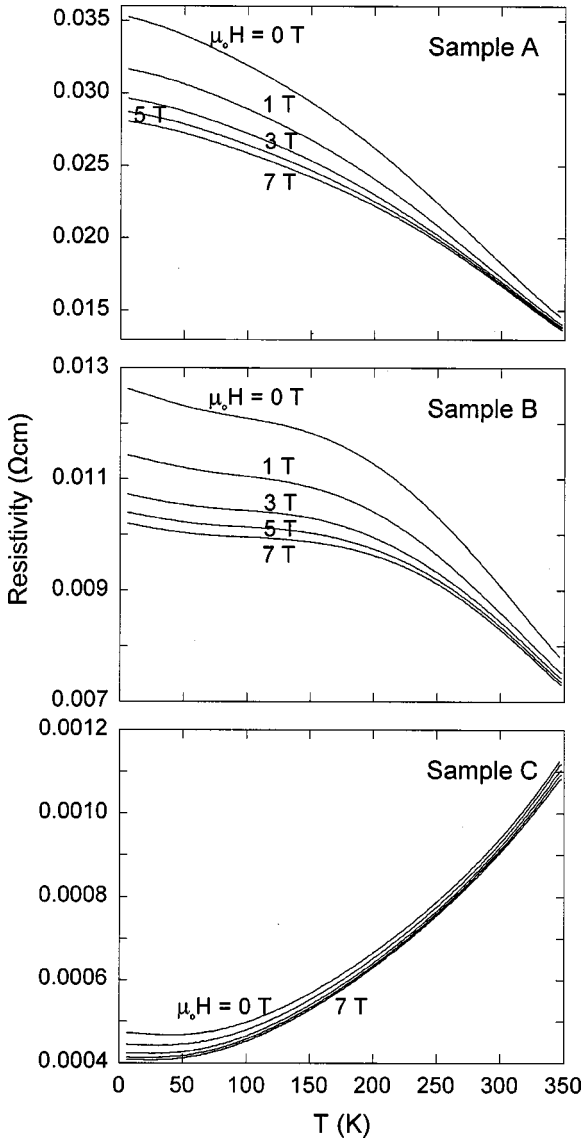

FIG. 1. Resistivity and magnetoresistive measurements as a function of temperature and applied magnetic field. At zero field, samples *A*, *B*, and *C* show insulating, semimetallic, and metallic properties, respectively.

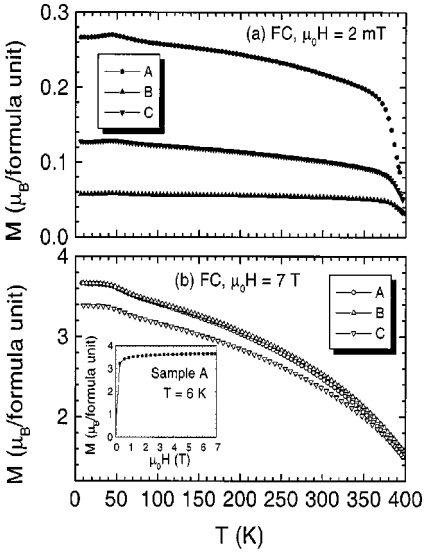

FIG. 2. Magnetization measurements for samples *A*, *B*, and *C* [at 2 mT (a) and at 7 T (b)] showing an effective moment in the range of $3.4-3.6\mu_B$ at 4.2 K (7 T). Magnetization measurements vs applied field (at 6 K, sample *A*) are shown in the inset of (b).

and *C*, respectively). From thermogravimetric (TGA) measurements, we observe a small variation in the oxygen content of up to ~0.18%, which may not explain (by itself) the dramatic differences in the conducting properties for these samples. Resistance measurements in fields up to 7 T showed a negligible magnetoresistance effect for the metallic sample *C* and a significant magnetoresistive response for samples *A* and *B* that increases with decreasing temperature (see Fig. 1). For sample *A*, the magnetoresistance effect {defined as $[\rho(T,H=0)-\rho(T,H)]/\rho(T,H)$} was calculated to be as large as 10% and 30% at room temperature and at 4.2 K, respectively, in good agreement with the results of Kobayashi *et al.*[1]

Magnetization measurements between 4.2 and 400 K and in fields of 2 mT and 7 T are shown in Figs. 2(a) and 2(b). Net moments of $\sim 3.4-3.6\mu_B$ were measured at 4.2 K (7 T) [Fig. 2(b)] consistent with the values reported in the literature for Sr_2FeMoO_6.[1–2,4,8] The small difference in magnetization measurements and magnetic transitions (with a T_c near 400 K for sample *A* and higher for samples *B* and *C*) suggests that there may be subtle differences in the compositions of the samples.

Neutron powder diffraction

Trace amounts of insulating $SrMoO_4$ (up to 5%) were seen in the neutron-diffraction patterns of samples *B* and *C* [see Fig. 3(a)]. Its structure[12] was included in the final refinements and is listed in Table II. At room temperature, all remaining neutron-diffraction peaks are accounted for with a tetragonal $\sqrt{2}a_p \times \sqrt{2}a_p \times \approx 2a_p$ unit cell. Neutron-diffraction measurements between 13 and 460 K for sample *A* show the splitting of several lines near T_c indicating a structural phase transition from cubic to tetragonal [see Fig. 3(b)].

The cubic structure of Sr_2FeMoO_6 can be described as a stack of ordered Fe and Mo octahedra that are connected to each other through shared corners. Sr, Fe, Mo, and O are at (1/4 1/4 1/4), (0 0 0), (1/2 0 0), and (*x* 0 0; where *x*

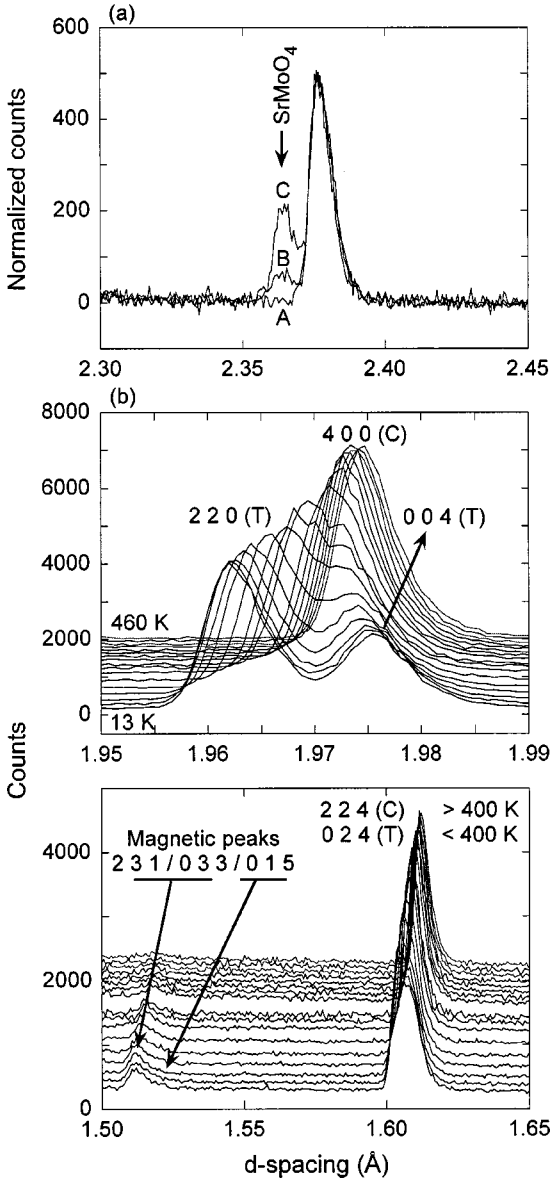

FIG. 3. (a) Portions of neutron powder diffraction patterns showing the presence of 0%, 2%, and 5% of $SrMoO_4$ impurity phase in samples *A*, *B*, and *C*, respectively. (b) Line splittings showing the cubic (*C*) to tetragonal (*T*) structural phase transition.

~0.251) positions, respectively. Oxygen atoms (occupying the corners of the octahedra) are therefore located on the edge of the unit cell between the octahedra.

At high temperature, above 420 K, the neutron powder diffraction data can be nicely fit using the cubic $Fm\bar{3}m$ model, as reported by García Landa *et al.*[8] The raw data and

TABLE II. Room-temperature (300 K) structural parameters for $SrMoO_4$. $a=5.3943(4)$ Å, $c=12.0436(16)$ Å, and volume$=350.45(5)$ Å^3. Tetragonal symmetry of space group $I4_1/a$.

Atom	*x*	*y*	*z*	*B* (Å^2)
Sr	0	1/4	1/8	0.5(3)
Mo	0	1/4	5/8	0.8(3)
O	0.244(2)	0.120(2)	0.043(1)	0.9(2)

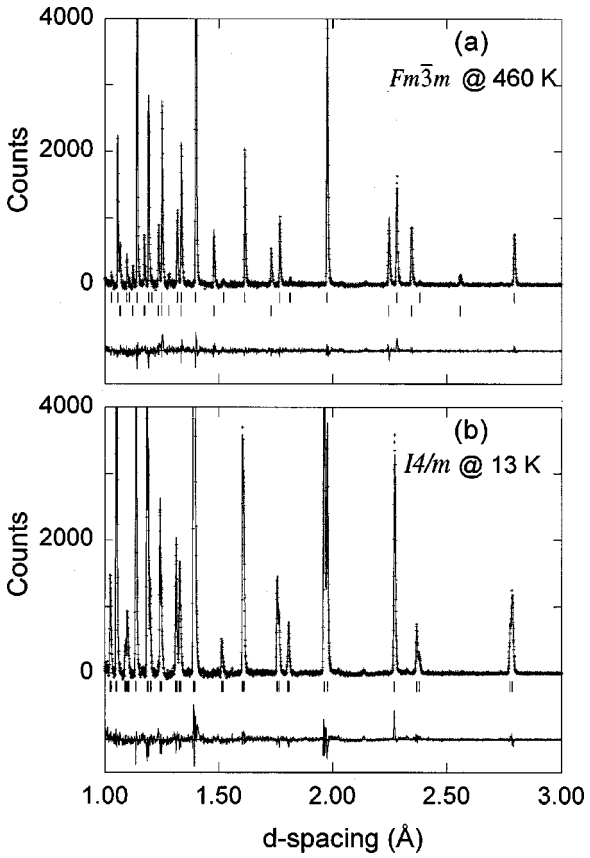

FIG. 4. Best-fit Rietveld profile using the space group $Fm\bar{3}m$ at 460 K (a) $I4/m$ at 13 K (b). Observed (plus signs) and calculated (solid line) intensities are shown together with their difference (at the bottom). At high temperature (above 300 K), the neutron-diffraction patterns contain extra peaks that belong to titanium (from the sample holder). The structure of titanium was included in the refinements. Tick marks below the patterns indicate the Bragg positions for Sr_2FeMoO_6 (top) and Ti (bottom; when present).

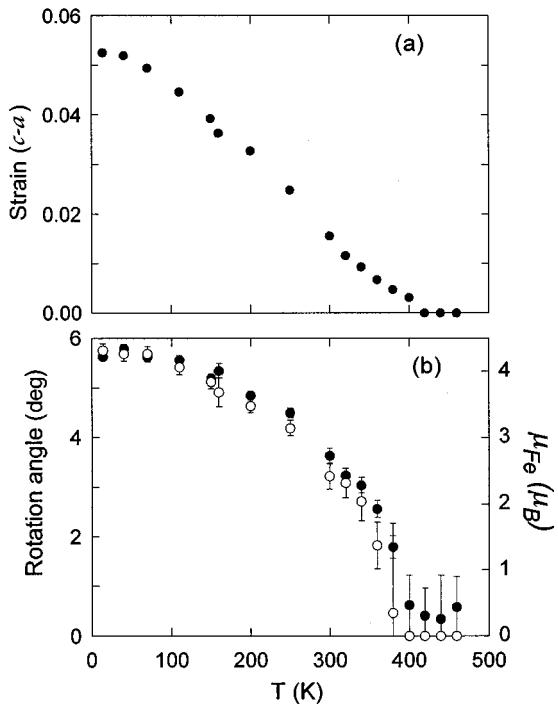

FIG. 5. (a) The tetragonal strain $(c-a)$ vs temperature showing the strain onset at ~420 K. (b) The rotation angle of the FeO_6 octahedra (open circles) and the refined magnetic moment for Fe (filled circles) as a function of temperature. The figure shows the remarkable scaling between the two parameters.

best-fit Rietveld profile are shown in Fig. 4(a). However, a tetragonal distortion, evidenced by selective peak broadening and, at lower temperatures, by peak splitting as shown in Fig. 3(b), is obvious below 420 K. At the lowest temperature, 13 K, a tetragonal $I4/m$ model provides an excellent fit to the data, establishing the structure of the phase below T_c. The raw data and best-fit Rietveld profile are shown in Fig. 4(b). The $I4/m$ tetragonal structure can evolve continuously from the $Fm\bar{3}m$ cubic structure with the simultaneous development of a tetragonal strain, $(c-a)$, and the rotation of FeO_6 octahedra. The transition is allowed to be continuous by both Landau theory and renormalization-group theory.[13]

The temperature dependencies of the strain and octahedral rotation are shown in Fig. 5. In our experimental data, the two order parameters, strain and rotation, appear to extrapolate to zero at slightly different temperatures, with the tetragonal strain remaining slightly nonzero above 400 K. We conclude that this is an artifact of the data perhaps resulting from a small amount of chemical inhomogeneity in our sample, which would smear the transition over a narrow range of temperatures and give rise to selective peak broadening, with tetragonal character, above the average transition temperature. Moreover, if the tetragonal strain were to develop while the rotation angle remained zero, this would imply a transition from $Fm\bar{3}m$ to $I4/mmm$, which is not allowed to be continuous,[13] followed by a subsequent transition to $I4/m$. The refined magnetic moment μ_{Fe} scales with the rotation angle and is nonzero only below 400 K.

For the results reported in this paper, the $Fm\bar{3}m$ model was used for refinement of data at $T \geqslant 420$ K and the $I4/m$ model was used for data at $T \leqslant 400$ K. We assign the transition temperature to be 400 K within the resolution of our experiment. Tables III and IV list the structural parameters and bond lengths at selected temperatures (460, 400, 300, and 70 K for insulating sample *A*) and at 300 K (for semimetallic sample *B* and metallic sample *C*).

Plots of the lattice parameters a and c (where a is multiplied by $\sqrt{2}$ in the tetragonal region), and the unit-cell volume (volume multiplied by 2 in the tetragonal region) as a function of temperature are shown in Fig. 6. As can be seen from Fig. 6(a), both the a and c axes change smoothly with decreasing temperature. However, the c axis exhibits a positive thermal expansion in the $Fm\bar{3}m$ phase and a negative thermal expansion in the $I4/m$ phase. Subtle changes are also seen around 380 K in the a axis and volume thermal expansion. The absence of abrupt changes (discontinuities) in all these structural parameters indicates that the structural phase transition is continuous.

In the cubic structure, Fe atoms have six equivalent Fe-O bonds of length ~1.995 Å and Mo atoms have six equivalent Mo-O bonds of length 1.956 Å (Fig. 7). Below the transformation temperature to the tetragonal $I4/m$ phase (~400 K) the four planar bonds for each cation initially contract at a rate faster than the average thermal contraction while the two apical bonds for each cation contract at a slower rate. As the

TABLE III. Structural parameters for Sr_2FeMoO_6: Sample *A* (insulating), Sample *B* (semimetallic), and Sample *C* (metallic).

		Sample *A*				Sample *B*	Sample *C*
Space Group		$Fm\bar{3}m$	$I4/m$	$I4/m$	$I4/m$	$I4/m$	$I4/m$
T (K)		460	400	70	300	300	300
a (Å)		7.89737(3)	5.58028(2)	5.55215(2)	5.57128(2)	5.57116(2)	5.56968(3)
c (Å)			7.89490(5)	7.90134(5)	7.89461(8)	7.89997(7)	7.89862(8)
c/*a*			1.41479	1.42311	1.41702	1.41801	1.41815
Vol. (Å^3)		492.546(6)	245.845(3)	243.570(3)	245.042(4)	245.198(2)	245.026(3)
Fe	*at* (0 0 0)						
	B (Å^2)	0.47(5)	0.50(5)	0.29(6)	0.31(6)	0.31(5)	0.28(5)
	n	0.99(1)	0.99(1)	0.99(1)	0.99(1)	0.99(1)	0.99(1)
	μ_x	0	0	3.5(1)	2.4(2)	2.6(1)	2.5(2)
	μ_z	0.4(4)	0.4(5)	2.5(2)	1.7(3)	1.4(3)	1.7(3)
	μ	0.4(4)	0.4(5)	4.29(7)	2.94(6)	2.97(5)	3.06(6)
Mo	*at* (0 0 1/2)						
	B (Å^2)	0.44(7)	0.30(18)	−0.08(6)	0.32(8)	0.35(6)	0.40(7)
	n	0.94(1)	0.94(1)	0.94(1)	0.94(1)	0.94(1)	0.95(1)
Sr	*at* (1/2 0 1/4)						
	B (Å^2)	1.02(2)	0.98(2)	0.30(1)	0.716(9)	0.729(7)	0.751(9)
O(1)	*at* (0 0 *z*)						
	z	0.2524(6)	0.252(4)	0.2542(8)	0.2528(9)	0.2519(7)	0.2516(8)
	B_{11}	0.58(8)	1.4(3)	0.54(3)	1.26(8)	1.16(5)	1.21(6)
	B_{22} (Å^2)	1.75(3)	1.4(3)	0.54(3)	1.26(8)	1.16(5)	1.21(6)
	B_{33}	1.75(3)	2.3(3)	0.27(6)	0.50(6)	0.50(5)	0.54(6)
O(2)	at (*x y* 0)						
	x		0.255(4)	0.2767(6)	0.2658(6)	0.2699(5)	0.2692(5)
	y		0.249(3)	0.2266(6)	0.2378(5)	0.2361(4)	0.2356(5)
	B_{11} (Å^2)		0.4(4)	−0.08(7)	0.4(1)	0.3(1)	0.3(1)
	B_{22}		0.8(6)	0.9(1)	1.0(1)	1.1(1)	1.2(1)
	B_{33}		2.4(3)	0.67(3)	1.34(5)	1.38(5)	1.36(5)
	B_{12}		−0.6(2)	−0.12(3)	−0.47(4)	−0.45(3)	−0.48(4)
χ^2		1.364	1.537	1.551	1.839	2.249	1.838
[a]R_{WP} (%)		5.17	4.78	6.22	5.77	5.28	6.25
[b]R_{F^2} (%)		7.20	5.30	4.05	4.53	4.54	4.66
R_{mag} (%)			14.36	4.74	4.39	4.03	4.57

[a]$R_{WP} = \sqrt{\Sigma w_i[y_i(\mathrm{obs}) - y_i(\mathrm{calc})]^2 / \Sigma w_i[y_i(\mathrm{obs})]^2}$, where $i = 1$, *n* and *n* is the number of observations, and y_i is the observed intensity.

[b]$R_{F^2} = \Sigma|I_K(\mathrm{obs}) - I_K(\mathrm{calc})| / \Sigma|I_K(\mathrm{obs})|$, where I_K is the assigned intensity to the *K*th Bragg reflection at the end of the refinements.

TABLE IV. Selected bond lengths for Sr_2FeMoO_6 (samples *A*, *B*, and *C*).

	Sample *A*				Sample *B*	Sample *C*
Space Group	$Fm\bar{3}m$	$I4/m$	$I4/m$	$I4/m$	$I4/m$	$I4/m$
T (K)	460	400	70	300	300	300
Fe-O(1)×2	1.994(4)	1.993(33)	2.009(6)	1.996(6)	1.990(5)	1.987(6)
Fe-O(2)×4	1.994(4)	1.992(16)	1.986(4)	1.987(4)	1.998(3)	1.992(4)
Mo-O(1)×2	1.956(4)	1.955(33)	1.942(6)	1.963(6)	1.960(5)	1.962(6)
Mo-O(2)×4	1.956(4)	1.956(16)	1.960(4)	1.951(4)	1.950(3)	1.955(4)
Sr-O(1)×4	2.79306(3)	2.79106(22)	2.77628(8)	2.78650(4)	2.78562(3)	2.78487(3)
Sr-O(2)×4	2.79306(3)	2.773(13)	2.6498(7)	2.7125(27)	2.6971(9)	2.6967(11)
Sr-O(2)×4	2.79306(3)	2.810(13)	2.9269(8)	2.8682(29)	2.8849(10)	2.8840(12)

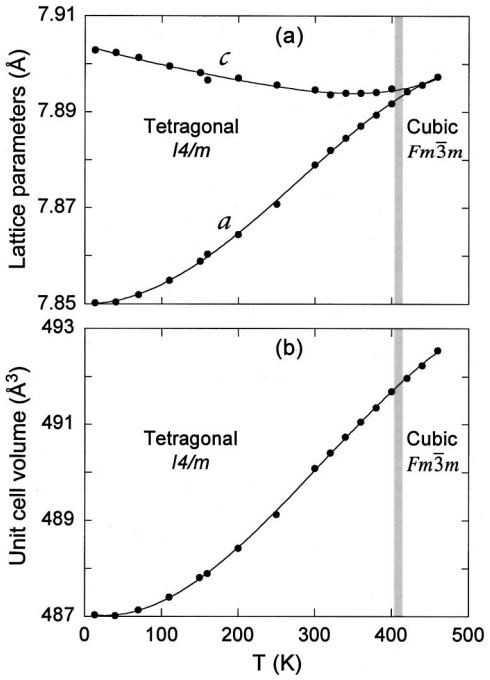

FIG. 6. Lattice parameters *a* and *c* (a) and unit-cell volume (b) as a function of temperature.

coordinated rotations of the corner-linked FeO_6 and MoO_6 octahedra grow, this allows the planar Fe-O and Mo-O bonds to maintain nominally constant lengths in spite of the thermal contraction. This is illustrated in Fig. 7. In the isostructural Ba_2FeMoO_6 compound, which has longer Fe-O bonds ($\sim$2.07 Å), the structure remains cubic at all temperatures.[14] This suggests that the Fe-O bond length of $\sim$1.995 Å in Sr_2FeMoO_6 is near the minimum that can be accommodated in this structure.

Even though samples *A*, *B*, and *C* exhibit significant differences in resistivity and magnetization, the structural differences are very subtle. Refined structural parameters for samples *B* and *C* at room temperature are compared to those for sample *A* in Table III. The c/a ratios (at 300 K), which are independent of systematic errors (e.g., resulting from sample positioning in the diffractometer) in a time-of-flight

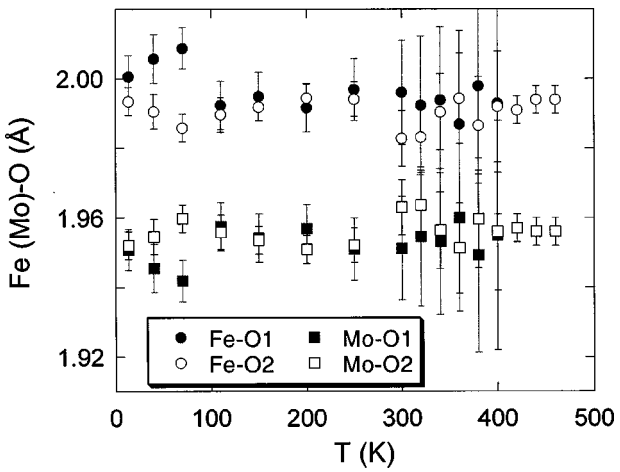

FIG. 7. Fe-O(1), Fe-O(2), Mo-O(1), and Mo-O(2) bond lengths as a function of temperature.

diffraction measurement, show a small but significant increase of $\sim$0.07% between samples *A* and *B*, and $\sim$0.01% between samples *B* and *C*. Such a small difference suggests that any differences in chemical composition must be very subtle. Refinement of site occupancies could provide insight concerning what defects exist that could account for sample differences. In the Rietveld refinements with our data, oxygen site occupancies refined to within one standard deviation of unity and were, thus, fixed at unity in the final refinements. The Fe and Mo site occupancies refined to 0.99(1) and 0.94(1), respectively, for samples *A* and *B* and 0.99(1) and 0.95(1) for sample *C*. Since Fe has a larger neutron-scattering cross section than Mo [$b(\mathrm{Fe})=0.954$ barns; $b(\mathrm{Mo})=0.695$ barns] the deficient scattering on the Mo site cannot result from Fe substitution on that site. Moreover, it is unlikely that Fe would substitute at the significantly smaller Mo site. We interpret the scattering deficiency as vacancies which may result from the high volatility of Mo during synthesis. The indication of a slight scattering deficiency on the Fe site could be interpreted as Mo substitution for Fe at the level of about 4%, but with an error bar as large as the value. Thus, we have no clear evidence for Fe/Mo disorder. The same conclusion holds for samples *B* and *C*, for which the refined site occupancies are given in Table III. Thus, within the sensitivity of our measurements, we cannot attribute the differences in these samples to obvious defects in the Sr_2FeMoO_6 structure. The differences in properties of bulk materials prepared in different ways could result from second phases in grain boundaries, as has been previously proposed.[4]

Ferrimagnetism of Sr_2FeMoO_6

The Sr_2FeMoO_6 double-perovskite structure consists of nominally Fe^{3+} and Mo^{5+} ions alternating in all three directions. In the simplest models for the magnetic structure, the magnetic moments of these ions can be ordered parallel, giving a ferromagnetic structure in which the moments add, or antiparallel, giving a ferrimagnetic structure in which the moment of Mo^{5+} is subtracted from that of Fe^{3+}. The expected magnetic moments are approximately $5\mu_B$ for Fe^{3+} and $1\mu_B$ for Mo^{5+}. Thus, the saturated net magnetic moment of $\sim 3.6\mu_B$ from magnetization measurements at 7 T [inset of Fig. 2(b)] seems to be consistent with a ferrimagnetic ordering model. Such a conclusion was suggested by Nakayama *et al.* in 1968 (Ref. 7) based on neutron powder diffraction data. However, in a more recent study, Garcia-Landa *et al.*[8] concluded that there was no ordered moment on the Mo ions and that the Fe ions exhibited an ordered moment of $4.1\mu_B$. They speculated that the lack of a magnetic moment on the Mo ions resulted from the itinerant nature of the spin down t_{2g} electrons.

In our neutron-diffraction data, we observe six significant magnetic Bragg intensities [indexed as 217/415, 341, 305/413, 231, 213, and 211/103 at 1.03, 1.10, 1.20, 1.51, 1.81, and $\sim$2.37 Å, respectively]. Since the perovskite unit cell is already doubled by the Fe/Mo ordering, all of these magnetic reflections are coincident with nuclear Bragg reflections. Selection rules do not define a unique magnetic structure. In general, the variable parameters in a model for the magnetic structure are the magnitudes and canting angles for the Fe

and Mo ions. Because of the small moment on Mo^{5+} and its form factor which falls off much more rapidly than for Fe^{3+}, we found that unconstrained refinements based on these four variables were too poorly determined to give a unique result. Refinements of the magnetic structure were, thus, done by comparing three possible models for the contribution of Mo and using only the data for $d \geq 1$ Å (while fixing all parameters that affect nuclear Bragg intensities). The three models assumed Mo ordered moments of $1\mu_B$ (ferromagnetic ordering), $-1\mu_B$ (ferrimagnetic ordering), and $0\mu_B$ (no ordered moment on Mo, as claimed by García-Landa *et al.*[8]). The weighted profile R values (R_{WP}) for these three refinements were 5.82%, 6.00%, and 5.90%, respectively. Thus, our data favor a ferrimagnetic ordering model, as concluded by Nakayama *et al.*[7] The ordered moment on Fe refined to $4.22\mu_B$, with a canting angle of 54° (with respect to the c axis) at 13 K. The canting of the Fe moments was clearly seen at temperatures below 320 K. Between 320 and 400 K, the observed magnetic peaks are weak and somewhat broad, making it difficult to refine the canting angle. At these temperatures, refinements were done with Fe moments aligned along the c axis. We do not have sufficient sensitivity to say whether the Fe moments are canted.

Using this model for the magnetic structure, the Mo and Fe magnetic moments were constrained as

$$\mu_{\mathrm{Mo}} = \frac{-1}{4.22}\mu_{\mathrm{Fe}}$$

and the total ordered moment for Fe was refined at each temperature giving the results plotted in Fig. 5(b). The refined magnetic moment appears to scale with the octahedral rotation angle and, in particular, goes to zero at the same temperature (within the precision of our measurements). This result shows that the magnetic ordering begins at the structural phase transition, ~400 K. The low-field magnetization measurements (Fig. 2) show a somewhat broad transition perhaps extending slightly above 400 K. We attribute this observation to chemical inhomogeneity of the sample which broadens the bulk magnetization transition (consistent with our observation of a small tetragonal peak broadening above 400 K).

Mössbauer spectroscopy

Mössbauer measurements were made at the ^{57}Fe nucleus in Sr_2FeMoO_6 over a temperature range of 10–460 K. Spectra obtained above T_c indicate a paramagnetic state [Fig. 8(a)], and spectra taken below T_c show the existence of magnetic ordering (Fig. 9). The neutron diffraction results suggest that two Fe environments should be seen: Fe in an undefected octahedral environment and Fe in the same crystallographic site but where a neighboring Mo site is vacant, giving a different Fe local environment. The two Fe sites are seen in the Mössbauer spectra at high temperature, above T_c, and at low temperature, 10 to 150 K. Two-site models have been used to fit the spectra in these temperature regions (Fig. 8).

A simple two-site Lorentzian fit (constraining the intensity ratio of the lines to 3:2:1:1:2:3) was made to the spectra at 10 K [Fig. 8(b)]. The main component (area about 70%), with narrow lines, was assigned to the Fe atoms occupying

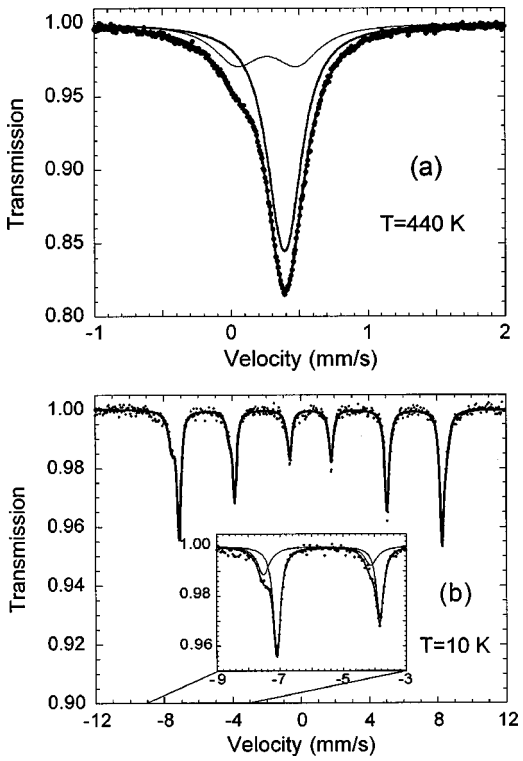

FIG. 8. Mössbauer spectra for sample A (insulating) of Sr_2FeMoO_6 obtained in the paramagnetic state (a) and below T_c at 10 K (b) where the existence of two magnetic components is shown (inset of b).

sites proper for an ordered double perovskite. The second component with a relative area of 30% may be assigned to a higher charge state of iron since it has a smaller shift, δ (where shift is defined as the sum of the chemical isomer shift and the thermal shift), and larger magnetic hyperfine field (Table V). This is thought to be due to the presence of Mo vacancies near the Fe site. Reduced electron density in

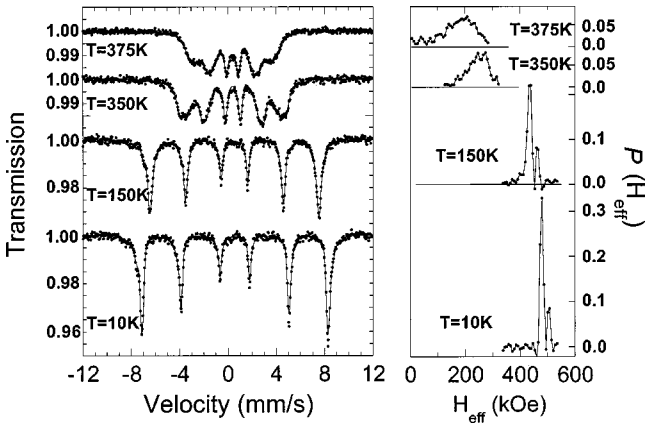

FIG. 9. Temperature dependence of Mössbauer spectra along with the distribution of magnetic hyperfine fields, $P(H_{\mathrm{eff}})$. In the fit to the data all Mössbauer lines were constrained to have the same Lorentzian linewidth and an ideal intensity ratio of 3:2:1:1:2:3, and each sextet of lines was constrained to have the same shift and quadrupole splitting.

TABLE V. Hyperfine parameters deduced from Mössbauer spectra for Sr_2FeMoO_6. For definition of the effective quadrupole splitting see text. Γ represents the half-width of the absorption line.

T (K)	Relative area	H_{eff} (kOe)	[a]δ (mm/s)	ε (mm/s)	Γ (mm/s)
10	$A_1=70\%$	477(1)	0.69(1)	0.02(1)	0.27(1)
	$A_2=30\%$	500(2)	0.61(1)	0.03(1)	0.45(1)
440	$A_1=69\%$		0.50(1)	0.06(2)	0.27(1)
	$A_2=31\%$		0.38(1)	0.45(1)	0.41(1)

[a]Shift with respect to iron metal.

the vicinity of Mo vacancies would cause an enhancement of the magnetic hyperfine field, and also decrease the shift.

Above T_c, at a temperature of 440 K, the spectrum also clearly reveals two components. Using the same two-site Lorentzian fit also gives relative area of about 70% and 30% for the two components. At this temperature, the second component was fit with a quadrupole doublet. The relative differences in the shift between the two components at 440 and 10 K are in reasonable agreement. The presence of the second component and its broad linewidth (0.41 mm/s) is again consistent with the presence of Mo vacancies which leads to local lattice distortions around the iron atoms. The main component has a narrow linewidth (0.27 mm/s) showing that it arises from sites having similar environments rather than having a distribution of environments caused by Mo vacancies.

The effective quadrupole splitting is defined as $\varepsilon(T>T_c)=eQV_{zz}/2$ and $\varepsilon(T<T_c)=eQV_{zz}(3\cos^2\theta-1)/4$ where Q is the quadrupole moment of the nucleus and θ is the angle between the principal axis V_{zz} of the electric-field gradient tensor and the direction of H_{eff}. When the local symmetry of the iron ion is less than cubic, a quadrupole interaction can split or shift the nuclear energy levels which is what is observed for the second component above T_c. However, if the second component is due to Mo vacancies, the angle between V_{zz} and H_{eff} will vary from one iron atom local environment to another. The term $(3\cos^2\theta-1)$ would have an average value of zero and the quadrupole splitting should then vanish below T_c (see Table V). The quadrupole splitting for the main component was almost zero above T_c (consistent with the cubic structure as seen by neutron diffraction), and below T_c. One may expect to observe quadrupole splitting for the tetragonal structure below T_c. However, from the neutron-diffraction results, the iron magnetic moments are found oriented to an angle of $\sim 54°$, with respect to the tetragonal c axis, resulting in a small value (~ 0.04) for the term $(3\cos^2\theta-1)$ and a negligible quadrupole splitting.

The relative areas of the two components are the same at 440 and 10 K (Table V) and are in good agreement with the concentration of Mo-site vacancies from neutron diffraction. A 6% probability of Mo vacancies (Table III) times 6 sites gives 36% probability that a Fe atom will be adjacent to a Mo vacancy, assuming that the Mo vacancies are randomly distributed.

Mössbauer spectroscopy is sensitive to the total magnetic moment at the iron site. Based on the calculations of Kobayashi *et al.*,[1] the total magnetic moment at the iron site should be $5\mu_B$ from the Fe-t_{2g} and Fe-e_g up-spin band below E_F minus the contribution of the moment arising from the overlap of the itinerant Mo-t_{2g} and Fe-t_{2g} down-spin band states. The total net moment at the iron site deduced from Mössbauer spectroscopy is $4.4\mu_B$, suggesting a net down $0.6\mu_B$ at the Fe site. The value of $4.4\mu_B$, which is in good agreement with neutron results, was obtained by using the two weighted mean hyperfine fields of the main and second component at 10 K (see Table V), assuming that one μ_B gives rise to 110 kOe.

At intermediate temperatures, ~ 150 K to T_c, the spectra are more complex (Fig. 9). Above 150 K a broad distribution of magnetic fields is observed which collapses at T_c (400 K for sample *A*) into the single sharp line and a broadened quadrupole doublet [Figs. 8(a), 9]. This behavior is straightforward to understand in terms of the defect structure. We propose that, because of the different Fe environments, magnetic ordering develops differently in the defected and undefected regions of the structure. Thus, at intermediate temperatures, a distribution of magnetic fields is seen at the Fe sites. At low temperature, where the magnetic ordering has saturated, the two distinct Fe sites (environments) are again seen.

Consistent with this physical picture, the spectra below T_c in the intermediate temperature region were fitted in terms of a distribution of magnetic hyperfine fields using the method of Wivel and Mørup.[15] In this method, the spectra were analyzed constraining all Mössbauer lines to have the same Lorentzian linewidth, shift, quadrupole splitting, and an ideal intensity ratio of 3:2:1:1:2:3. The resulting curves $P(H_{\text{eff}})$, where H_{eff} is the magnetic hyperfine field, are shown in Fig. 9 for sample *A*. Below 150 K, there are two well-resolved distribution peaks; thus the spectra below 150 K are essentially composed of two distinct components. Above 300 K, $P(H_{\text{eff}})$ evolves into a broad distribution of magnetic fields as the temperature approaches T_c. The significant line broadening appears to be a feature characteristic of many perovskites.[2,3,9,16–18] Linden *et al.*[19] recently published very similar Mössbauer data for the same compound, in which they observed evidence for a distribution of magnetic fields at intermediate temperatures.

For sample *A*, the ordering temperature, T_c, was determined to be ~ 400 K from the temperature dependence of $\langle H_{\text{eff}}\rangle$, the mean magnetic hyperfine field, in good agreement with the neutron-diffraction results (Fig. 10). The temperature variation of the average shift is that expected if it were mainly due to the second-order doppler shift (Fig. 10 inset).[20] The small kink near T_c is indicative of a second-order phase transition which is in agreement with the neutron-diffraction results. The spectra obtained for the three samples *A*, *B*, and *C* having different conductivity properties (insulating, semimetallic, and metallic) were found to be similar to each other.

The hyperfine parameters most sensitive to the valence state of iron are the shift, δ, of the resonance spectrum and the mean magnetic hyperfine field $\langle H_{\text{eff}}\rangle$ at the nuclear site. The screening by the $3d$ shell electrons of $3s$ and $4s$ electrons at the nucleus gives rise to a dependence of the shift upon the $3d$ population. Generally, the shift decreases with increasing charge-state of iron. Typical ranges of shifts found in iron compounds at room temperature are $+0.3$ to $+0.6$ mm/s and $+0.8$ to $+1.5$ mm/s for high-spin Fe^{3+} and

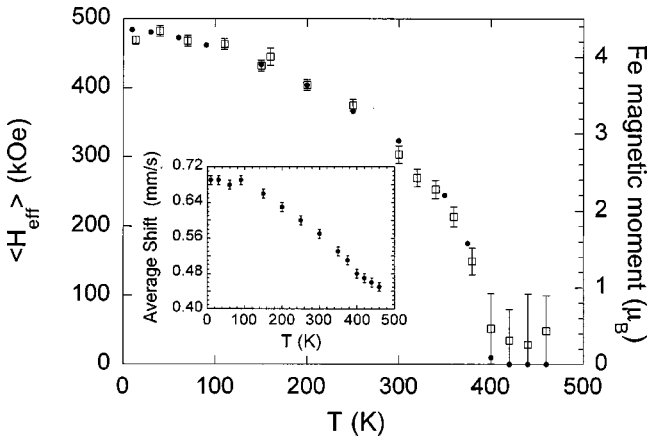

FIG. 10. The mean magnetic hyperfine field $\langle H_{\mathrm{eff}}\rangle$ (filled circles) and the magnetic moment of Fe, determined from neutron diffraction (open squares), as a function of temperature. The inset shows the variation of the shift δ (relative to iron) with temperature.

Fe^{+2}, respectively.[21,22] In ionic compounds the most significant term which contributes to the magnetic hyperfine field is the Fermi contact interaction. Its value is proportional to the mean spin $\langle S_z\rangle$ of the $3d$ electrons. For high-spin ions the values of $\langle S_z\rangle$ are 5/2 and 2 for Fe^{+3} and Fe^{+2}, respectively. At low temperatures the Fermi contact term is about 550 kOe for the Fe^{+3} and about 440 kOe for Fe^{+2}, which corresponds to 110 kOe per Bohr magneton.

The mean magnetic field at low temperatures was found to be intermediate between that for Fe^{+3} and Fe^{+2} (see Fig. 10). The average shift was also found to be intermediate between high-spin configuration values of Fe^{+3} and Fe^{+2}. For example, the Mössbauer spectrum at room temperature has a shift $\delta = 0.58(1)$ mm/s, which is close to the intermediate valence state $Fe^{+2.5}$ ($\delta = 0.67$ mm/s) for the B sites in Fe_3O_4.[21,23] The octahedral B sites in Fe_3O_4 have distinct states of Fe^{+3} and Fe^{+2} below the Verwey transition, but above the Verwey transition fast electron hopping occurs between Fe^{+3} and Fe^{+2} resulting in the intermediate valence state and shift measured. In a recent paper, Linden *et al.*[19] have also concluded from Mössbauer data for Sr_2FeMoO_6 that Fe has an intermediate valence state and that there is no Verwey transition in this compound. The intermediate shift measured for Sr_2FeMoO_6 is consistent with the metallic-like, bulk behavior observed in these compounds[2–4,16,24] and the semimetallic state model calculated for this compound by Kobayashi *et al.*[1] and measured by optical conductivity by Tomioka *et al.*[24] The density of states obtained by this calculation show that the up-spin band, placed below the Fermi level, is mainly occupied by 5 Fe $3d$ electrons forming localized spins on the Fe sites. The down-spin band which has density of states at the Fermi level is composed mainly of hybridized Mo $4d\ t_{2g}$ and Fe $3d\ t_{2g}$ states. Thus, the Mo electron which occupies the down-spin band is itinerant and is shared among the Fe and Mo sites.

CONCLUSIONS

The nuclear and magnetic structures of Sr_2FeMoO_6 have been investigated using neutron powder diffraction and Mössbauer spectroscopy at temperatures between 10 and 460 K. Fe and Mo atoms are found to order on alternate sites, as expected, giving rise to a double-perovskite type unit cell. From 460 to 400 K, the structure of Sr_2FeMoO_6 is cubic of space group $Fm\bar{3}m$. A structural phase transition takes place from cubic to tetragonal $I4/m$ at ~400 K. In the tetragonal structure, the Fe and Mo octahedra rotate around the c axis by an angle of up to ~5.6°. Below the transition temperature T_c, the magnetic moments of Fe first align along the c direction and then rotate, as the temperature is lowered, to an angle of ~54° with respect to the c axis. The refined magnetic moment for Fe saturates at $\sim 4.3\mu_B$ at the lowest temperatures. Our neutron diffraction data indicate the presence of about 6% of vacancies on the Mo sites and give evidence for the ferrimagnetic ordering of the Fe and Mo magnetic moments.

Mössbauer spectroscopy was used to probe the local magnetic and electronic properties of Sr_2FeMoO_6. Two components are found at low and high temperatures. The relative areas of the two components are consistent with the 6% Mo vacancy concentration seen by neutron diffraction. The temperature dependence of the mean hyperfine field is in good agreement with the neutron-diffraction results and gives the same transition temperature. The mean hyperfine field yields a magnetic moment of $4.4\mu_B$ also in agreement with the neutron-diffraction results. From the shift measurements, the average valence of Fe is found to be intermediate between the high-spin configuration values of Fe^{+3} and Fe^{+2}.

ACKNOWLEDGMENTS

We wish to thank Hagai Shaked for useful discussions and Simine Short for her technical support. Work at NIU was supported by the ARPA/ONR and by the State of Illinois under HECA. At ANL, this work was supported by the U.S. Department of Energy, Office of Science, under Contract No. W-31-109-ENG-38.

[1] K.-I. Kobayashi, T. Kimura, H. Sawada, K. Terakura, and Y. Tokura, Nature (London) **395**, 677 (1998).
[2] T. Nakagawa, J. Phys. Soc. Jpn. **24**, 806 (1968).
[3] T. Nakagawa, K. Yoshikawa, and S. Nomura, J. Phys. Soc. Jpn. **27**, 880 (1969).
[4] M. Itoh, I. Ohta, and Y. Inaguma, Mater. Sci. Eng., B **41**, 55 (1996).
[5] F. S. Galasso, F. C. Douglas, and R. J. Kasper, J. Chem. Phys. **44**, 1672 (1966).
[6] T. Nakamura, K. Kunihara, and Y. Hirose, Mater. Res. Bull. **16**, 321 (1981).
[7] S. Nakayama, T. Nakagawa, and S. Nomura, J. Phys. Soc. Jpn. **24**, 219 (1968).
[8] B. García-Landa, C. Ritter, M. R. Ibarra, J. Blasco, P. A. Algarabel, R. Mahendiran, and J. García, Solid State Commun. **110**, 435 (1999).
[9] A. W. Sleight and J. F. Weiher, J. Phys. Chem. Solids **33**, 679 (1972).

[10] J. D. Jorgensen, J. J. Faber, J. M. Carpenter, R. K. Crawford, J. R. Haumann, R. L. Hitterman, R. Kleb, G. E. Ostrowski, F. J. Rotella, and T. G. Worton, J. Appl. Crystallogr. **22**, 321 (1989).
[11] A. C. Larson and R. B. von Dreele, General Structure Analysis System, University of California, 1985–1990.
[12] P. P. Ewald and C. Hermann, Strukturbericht, pp. 347–349 (1913–1926).
[13] H. T. Stokes and D. M. Hatch, *Isotropy Subgroups of the 230 Crystallographic Space Groups* (World Scientific, Singapore, 1988), pp. 1–371.
[14] O. Chmaissem *et al.* (unpublished).
[15] C. Wivel and S. Morøp, J. Phys. E **14**, 605 (1981).
[16] K. Shono, M. Abe, M. Gomi, and S. Nomura, J. Phys. Soc. Jpn. **21**, 1720 (1982).
[17] V. Chechersky, A. Nath, I. Isaac, J. P. Franck, K. Ghosh, and R. L. Greene, J. Phys.: Condens. Matter **11**, 8921 (1999).
[18] A. Tkachuk, K. Rogacki, D. E. Brown, B. Dabrowski, A. J. Fedro, C. W. Kimball, B. Pyles, X. Xiong, and D. Rosenmann, Phys. Rev. B **57**, 8509 (1998).
[19] J. Linden, T. Yamamoto, M. Karppinen, and H. Yamauchi, Appl. Phys. Lett. **20**, 2925 (2000).
[20] B. Kolk, in *Dynamical Properties of Solids*, edited by G. K. Horton and A. A. Maradudh (North-Holland, New York, 1984), Vol. 5.
[21] N. N. Greenwood and T. C. Gibb, *Mössbauer Spectroscopy* (Chapman and Hall, London, 1971).
[22] W. M. Reiff, in *Mössbauer Effect Methodology*, edited by I. J. Gruverman and C. W. Seidel (Plenum, New York, 1973) Vol. 8, pp. 89-106
[23] M. Sorescu, D. Mihaila-Tarabasanu, and L. Diamandescu, Appl. Phys. Lett. **72**, 2047 (1998).
[24] Y. Tomioka, T. Okuda, Y. Okimoto, R. Kumai, and K.-I. Kobayashi, Phys. Rev. B **61**, 422 (2000).